PtM/C Catalyst Prepared Using Reverse Micelle Method for Oxygen Reduction Reaction in PEM Fuel Cells

Yangdong Qian,*,†,‡ Wen Wen,†,§ Peter A. Adcock,† Zheng Jiang,‡ Nazih Hakim,† Madhu S. Saha,† and Sanjeev Mukerjee*,†

Department of Chemistry, Northeastern University, 360 Huntington Avenue, Boston, Massachusetts 02115, Inorganic Chemistry Laboratory, Wolfson Catalysis Center, University of Oxford, OX1, 3QR, U.K., and Department of Chemistry, Brookhaven National Laboratory, Upton, New York 11973

Received: June 25, 2007; In Final Form: October 8, 2007

Synthesis of carbon-supported PtM/C catalysts (M = Co, Cr, or Fe) using a new preparation technique, a reverse micelle method, is reported. The catalysts were characterized by different surface techniques: X-ray diffraction, scanning electron microscope, transmission electron microscope, and energy dispersive X-ray microanalysis. Surface characterization showed that Pt/M nanoparticles on catalysts were synthesized using the reverse micelle method. Pt/M nanoparticles were observed to be uniform spherical objects. The performance of the PtM/C catalysts was tested by the rotating disk electrode technique. A trend of catalytic activity for oxygen reduction reaction (ORR) was obtained: PtCo/C(T, 500) ∼ PtCo/C(S) > PtCr/C(S) > PtFe/C(S) ∼ Pt/C > PtFe/C(T, 500) ∼ PtCr/C(T, 500), showing that PtCo/C-type catalysts had a higher catalytic activity for ORR.

Introduction

One of the main obstacles to the highly successful application in transportation markets of proton exchange membrane (PEM) fuel cells is low performance of the oxygen reduction reaction at the cathode. Although expensive platinum-based catalysts seem to be the best catalyst for the oxygen reduction reaction at the cathode so far, they are still at least 10^6 times less active for oxygen reduction than for H_2 oxidation at the anode.[1] This leads to high overpotentials and is the major catalytic limitation to PEM fuel cell efficiency. Therefore, it is very important to improve catalytic performance of oxygen reduction and decrease the amount of platinum in catalysts. To obtain the optimum utilization of Pt, it is generally dispersed as small particles on a conductive support, such as high-surface-area carbon powders.[2,3] Carbon-supported Pt has proven to be the most active and durable catalyst for oxygen reduction. However, at reasonable current densities, Pt still shows overpotentials of 400 mV from the equilibrium reversible potentials (1.2 V at 80 °C). Therefore, great efforts have been made to identify and develop superior Pt catalysts for oxygen reduction. Many studies have reported that platinum alloy catalysts have been found to display increased catalytic activity for oxygen reduction.[4−6] These nanodispersed particles of Pt alloys were found to show improved intrinsic activity and stability over pure Pt.[1,7−17] The Pt alloy is formed between Pt surface of Pt/C and transition metals such as Fe, Ni, Co, Cr, etc. The techniques reported for the preparation of carbon-supported Pt-based alloy catalysts include the traditional methods, such as impregnation[1,17] and precipitation.[1,18] These traditional methods have the disadvantage of particle sintering due to the high temperature (over 900 °C) required to form the alloy, resulting in a lower catalyst active area.[1] Another disadvantage of these traditional methods is that the two metals may deposit at separate sites on the carbon, rather than in close association.

Recently, Sun reported synthesis of monodisperse iron−platinum (FePt) nanoparticles by reduction of platinum acetylacetonate and decomposition of iron pentacarbonyl in the presence of oleic acid and oleyl amine stabilizers.[19,20] Zhang obtained platinum−cobalt nanoparticles using a water-in-oil reverse microemulsion of water−Triton X-100−propan-2-ol−cyclohexane.[21] Well-dispersed Pt−Ru/C nanoparticles were synthesized using the surfactant tetraalkylamonium bromide by Schmidt and Paulus.[22,23] The above-mentioned preparation methods of nanoparticles are called water-in-oil microemulsion media or a reverse micelle (RM) method. In a reverse micelle, the polar groups of the surfactants are concentrated in the interior and the lipophilic groups extend toward and into the nonpolar solvent. Reverse micelles consist of nanometer-sized water droplets that are dispersed in an oil medium and stabilized by surfactants. These reverse micelle systems are heterogeneous on a molecular scale; nevertheless, they are thermodynamically stable. Reverse micelle systems are suitable reaction media for the synthesis of nanoparticles because tiny droplets of water are encapsulated into reverse micelles. Water pools of these reverse micelles act as microreactors for performing simple reactions of synthesis, and the size of microcrystals of the product is determined by the size of these pools. The size of the water pools is known to be controlled by the molar water/surfactant ratio in the system. Varying the water/surfactant ratio can form different size micelles, thus leading to careful control over the particle size. A cosurfactant is used to help decrease the fraction of the micelle head group that is neutralized and thereby increase the stability of the micelle. Without the addition of the cosurfactant, the amount of free water available to carry

* Corresponding authors. (Y.Q.) Tel: +44-1235-841716. Fax: +44-1235-841700. E-mail: yangdong.qian@oxfordcatalysts.com. (S.M.) Tel: 617-373-2382. Fax: 617-373-8949. E-mail: s.mukerjee@neu.edu.

† Northeastern University.

‡ University of Oxford.

§ Brookhaven National Laboratory.

10.1021/jp074929i CCC: $40.75
Published on Web 01/08/2008

TABLE 1: Components of Reverse Micelle Systems in Simultaneous Reaction Procedure

	catalyst		
	PtCo/C	PtCr/C	PtFe/C
	Reverse Micelle (I)		
aqueous phase	0.5 M H_2PtCl_6, 4.0 mL 1.0 M $CoCl_2$, 2.0 mL	0.5 M H_2PtCl_6, 4.0 mL 1.0 M $Cr(NO_3)_3$, 2.0 mL	0.5 M H_2PtCl_6, 4.0 mL 1.0 M $Cr(NO_3)_3$, 2.0 mL
surfactant	AOT, 9 g	AOT, 9 g	AOT, 9 g
cosurfactant	1-butanol, 9 g	1-butanol, 9 g	1-butanol, 9 g
oil phase	cyclohexane, 27 g	cyclohexane, 27 g	cyclohexane, 27 g
	Reverse Micelle (II)		
aqueous phase	2.0 M $NaBH_4$, 10 mL	2.0 M $NaBH_4$, 10 mL	2.0 M $NaBH_4$, 10 mL
surfactant	AOT, 9 g	AOT, 9 g	AOT, 9 g
cosurfactant	1-butanol, 9 g	1-butanol, 9 g	1-butanol, 9 g
oil phase	cyclohexane, 27 g	cyclohexane, 27 g	cyclohexane, 27 g

TABLE 2: Components of Reverse Micelle Systems in Sequential Reaction Procedure

		catalyst		
		PtCo/C	PtCr/C	PtFe/C
reverse micelle (I)	aqueous phase	1.0 M $CoCl_2$ (2.0 mL)	1.0 M $Cr(NO_3)_3$ (2.0 mL)	1.0 M ($FeCl_3$) (2.0 mL)
	surfactant	AOT, 5 g	AOT, 5 g	AOT, 5 g
	cosurfactant	1-butanol, 5 g	1-butanol, 5 g	1-butanol, 5 g
	oil phase	cyclohexane, 15 g	cyclohexane, 15 g	cyclohexane, 15 g
reverse micelle (II)	aqueous phase	2.0 M $NaBH_4$ (3.0 mL)	2.0 M $NaBH_4$ (4.0 mL)	2.0 M $NaBH_4$ (4.0 mL)
	surfactant	AOT, 5 g	AOT, 5 g	AOT, 5 g
	cosurfactant	1-butanol, 5 g	1-butanol, 5 g	1-butanol, 5 g
	oil phase	cyclohexane, 15 g	cyclohexane, 15 g	cyclohexane, 15 g
reverse micelle (III)	aqueous phase	0.5 M H_2PtCl_6 (4.0 mL)	0.5 M H_2PtCl_6 (4.0 mL)	0.5 M H_2PtCl_6 (4.0 mL)
	surfactant	AOT, 5 g	AOT, 5 g	AOT, 5 g
	cosurfactant	1-butanol, 5 g	1-butanol, 5 g	1-butanol, 5 g
	oil phase	cyclohexane, 15 g	cyclohexane, 15 g	cyclohexane, 15 g
reverse micelle (IV)	aqueous phase	2.0 M $NaBH_4$ (6.0 mL)	2.0 M $NaBH_4$ (6.0 mL)	2.0 M $NaBH_4$ (6.0 mL)
	surfactant	AOT, 5 g	AOT, 5 g	AOT, 5 g
	cosurfactant	1-butanol, 5 g	1-butanol, 5 g	1-butanol, 5 g
	oil phase	cyclohexane, 15 g	cyclohexane, 15 g	cyclohexane, 15 g

on the reactions is greatly reduced because most of the water is locked in the head group of the surfactant.[24] The reverse micelle method is used to make perfect particle control over particle size and uniformity be practicable. On the other hand, it does not require extremely high temperature and pressure conditions or any special equipment. The reverse micelle method is widely used in production of metallic nanoparticles, semiconductor materials, and nanometer-scale magnetic particles.[25−29] Bonnemann has proved that the reverse micelle method is a good way to prepare nanometer-scale catalysts.[25]

In the experiments reported in this paper, we prepared PtM (M = Co, Cr, or Fe) nanoparticles using a reverse micelle method, then deposited those PtM nanoparticles on carbon (Ketjen Black) to obtain PtM/C catalysts. Two reaction procedures, simultaneous reduction and sequential reduction in the reverse micelle methods, were used to observe if the catalytic activity of the oxygen reduction reaction was varied. Catalysts were characterized using X-ray diffraction (XRD), a transmission electron microscope (TEM), and scanning electron microscopy/energy-dispersive X-ray microanalysis (SEM/EDX). A rotating disk electrode (RDE) was used to observe the catalytic activity of the oxygen reduction reaction.

Experimental Methods

Synthesis of PtM Nanoparticle. All syntheses of carbon-supported PtM catalysts were carried out in an argon atmosphere using a Schlenk technique. Sodium dioctyl sulfosuccinate (AOT) was purchased from Fisher Scientific. All other chemicals were obtained from Aldrich. Reverse micelle solutions consisted of an oil phase cyclohexane, surfactant AOT, and cosurfactant 1-butanol. An aqueous phase containing the reactants H_2PtCl_6 and $CoCl_2$ ($Cr(NO_3)_3$ or $FeCl_3$) were used to form the reverse micelle. Another aqueous phase containing the reducing agent $NaBH_4$ was also used to form another reverse micelle. The PtM nanoparticles were prepared by a simultaneous reduction or sequential reduction procedure. Components of reverse micelle systems for the experiment are indicated in Tables 1 and 2.

The simultaneous reaction procedure was a two-emulsion technique (Table 1). A 9 g portion of AOT, 9 g of 1-butanol, 27 g of cyclohexane, 4 mL of 0.5 M H_2PtCl_6, and 2.0 mL of 1 M $CoCl_2$ ($Cr(NO_3)_3$ or $FeCl_3$) solution were added in a 300 mL, three-neck flask reactor under Ar atmospheric conditions, and the mixture was stirred at room temperature for 30 min to form the reverse micelle (I). The color of the solution is orange, reflecting the mixed color of the $PtCl_6^{2-}$ and Co^{2+} (Cr^{3+} or Fe^{3+}) ions. A 9 g portion ofAOT, 9 g of 1-butanol, 27 g of cyclohexane, and 10 mL of 2 M $NaBH_4$ were added in a flask (this solution is colorless) under Ar atmospheric conditions to form a reverse micelle (II). The reverse micelle (II) was then transferred into the reverse micelle (I). PtM nanoparticles were formed when H_2PtCl_6−$CoCl_2$ ($Cr(NO_3)_3$ or $FeCl_3$) solution and reducing solution $NaBH_4$ contacted each other. The color of the solution changed to dark from orange due to the suspended reduced metal nanoparticles. The reaction was allowed to mix for 2 h under Ar. Pure Pt nanoparticles were made by the same procedure without the $CoCl_2$ ($Cr(NO_3)_3$ or $FeCl_3$) solution.

A sequential reaction procedure was a four-emulsion technique (Table 2). A 5 g portion of AOT, 5 g of 1-butanol, 15 g of cyclohexane, and 2.0 mL of 1 M $CoCl_2$ ($Cr(NO_3)_3$ or $FeCl_3$) solution was added to a 300 mL, three-neck flask under Ar atmospheric conditions, and the mixture was stirred at room temperature for 30 min to form the reverse micelle (I). The color of the solutions is pink, violet, or light orange, reflecting the color of Co^{2+}, Cr^{3+}, or Fe^{3+}ions, respectively. A 5 g portion of

TABLE 3: Catalysts Prepared Using Reverse Micelle

catalyst	preparation methods	Pt wt %	Pt/M (atomic)
Pt/C	simultaneous	44%	
PtCo/C(S)	simultaneous	37%	64:36
PtCo/C(T)	sequential	40%	61:39
PtCr/C(S)	simultaneous	42%	90:10
PtCr/C(T)	sequential	38%	74:26
PtFe/C(S)	simultaneous	42%	85:15
PtFe/C(T)	sequential	37%	24:76

AOT, 5 g of 1-butanol, 15 g of cyclohexane, and 3 mL of 2 M $NaBH_4$ was added to a flask (this solution is a colorless) under Ar atmospheric conditions to form the reverse micelle (II). The reverse micelle (II) was then transferred into the reverse micelle (I). M nanoparticles were formed when $CoCl_2$ ($Cr(NO_3)_3$ or $FeCl_3$) solution and reducing solution $NaBH_4$ contacted each other. The color of the solution changed to gray from pink, violet, or light orange due to the suspended reduced M nanoparticles. The reaction was allowed to mix for 30 min under Ar. A 5 g portion of AOT, 5 g (6.5 mL) of 1-butanol, 15 g (20 mL) of cyclohexane, and 0.5 M H_2PtCl_6 (4.0 mL) solution was added to a flask under Ar atmospheric conditions, and the mixture was stirred at room temperature for 30 min to form the reverse micelle (III). The reverse micelle (III) was added into the above three-neck flask reactor under Ar atmospheric conditions and stirred at room temperature for 30 min. A 5 g portion of AOT, 5 g of 1-butanol, 15 g of cyclohexane, and 6 mL of 2 M $NaBH_4$ was added to a flask (this solution is colorless) under Ar atmospheric conditions and the mixture was stirred at room temperature for 30 min to form the reverse micelle (IV). The reverse micelle (IV) was transferred into the above reactor. Pt-coated M nanoparticles were formed when the H_2PtCl_4 solution and the reducing solution $NaBH_4$ contacted each other in the presence of the oil phase containing the M nanoparticles. The color of the solution changed to dark from gray due to the suspended reduced Pt-coated M nanoparticles. The reaction was allowed to mix for 1.5 h under Ar.

Preparation of Carbon-Supported PtM Catalysts. The appropriate amount of carbon (Ketjen Black), dispersed in cyclohexane under ultrasonic wave agitation for 30 min, was added to the above micelle solution containing PtM nanoparticles under constant stirring over 8 h (or overnight). A 50 mL portion of ethanol was then added to this mixture to break this reverse micelle, and the mixture was allowed to continue to stir 30 min; the supported carbon precipitated. The precipitate was filtered using a submicrometer-pore-sized filter (0.22 μm Millipore filter). After washing with 1:1 water and ethanol, cyclohexane and acetone, the product was dried at 120−140 °C under vacuum over 8 h (or overnight). Pure Pt/C was prepared by the same procedure but with only Pt nanoparticles. The content of the Pt metal was approximately 40 wt % in the catalysts. Carbon-supported PtM/C catalysts were loaded into a silica tube and heated in hydrogen gas at a ramp rate of 5 °C min^{-1} to the desired temperature (200 or 500 °C) and held at this temperature for 1 h, then passed through argon for 1 h and cooled to room temperature. These catalysts are denoted as PtM/C(T, 200), PtM/C(T, 500), PtM/C(S, 200), and PtM/C(S, 500), respectively. Table 3 shows all catalysts prepared by the reverse micelle method.

Surface Characterization. Powder XRD patterns of the catalysts were collected using a Philips X-ray diffractometer. The catalyst samples were held on an Al sample holder. An incident beam of X-rays of wavelength 1.5418 Å (CuK_α) filtered by a nickel filter was used. The samples were scanned from $10° < 2\theta < 90°$. The recorded patterns were matched against existing powder patterns using the JCPDS files. The average size of the sample crystallite may be estimated by the Debye−Scherrer equation.[30]

The morphologies of carbon and metal particles were obtained using a field emission scanning electron microscope (FE SEM, Hitachi S-4800 SEM) and transmission electron microscope (JEOL 2000fx). The composition analysis of the catalysts was carried out using energy-dispersive X-ray microanalysis. A small amount of Pt/C or PtM/C electrocatalyst sample was added to a glass ampule containing 2-propanol and placed in an ultrasonic bath for approximately 10 min. A drop of the suspension was pipetted onto a carbon-coated copper grid (3 mm, 200 mesh), and the solvent was allowed to evaporate from the grid. The grid was then placed into the microscope. The elemental distribution of the EDX spectrum was carried out using a computer program. The size of the metal particles was measured by Photoshop 7.0 image software.

Rotating Disk Electrode. Rotating disk electrode experiments were carried out at room temperature using a Pine Instrument Analytical Rotator and Voltalab-10 system. The glassy carbon rotating disk electrode (GC RDE, Pine Instrument) was polished with a 0.05 μm alumina suspension on a polishing cloth and then cleaned in distilled water for use as a support for the catalyst layer. The geometric surface area of the GC RDE is 0.196 cm^2 (diameter 5 mm). Perchloric acid (70%, analytical grade) was diluted with distilled water to prepare 1 M $HClO_4$. A catalyst containing 5.448 mg of Pt was added to 20 mL of IPA and 80 μL of 5 wt % Nafion, and the mixture was ultrasonically dispersed to get a catalyst ink. A 15 μL portion of catalyst ink was pipetted onto the GC RDE surface to get a Pt loading of ~21 μg Pt/cm^2 and allowed to dry before starting the RDE experiments.

The glass cell was cleaned by soaking in a 1:1 mixture of concentrated HNO_3 and H_2SO_4, followed by thorough rinsing with high-purity water. The counter electrode was a Pt wire, and the reference electrode was a sealed reversible hydrogen electrode (RHE) made from the same concentration of the electrolyte used in the experiment. All potentials were referred to the RHE. Cyclic voltammograms for the catalyst layers were recorded in 1 M $HClO_4$ at room temperature. The potential was scanned between 0 and 1.2 V at a scan rate of 50 mV s^{-1}. Before recording, the potential was repeatedly scanned in the same range to remove residual impurities. Current−potential relations were measured in O_2-saturated 1 M $HClO_4$ at room temperature at various rotation speeds. The scan rate of the potential was fixed at 25 mV s^{-1}. The potential was finally stepped to 0.2 V and then swept in the positive direction from 0.2 to 1.2 V to obtain a current−potential relationship. The potential was also swept in the negative direction in the same range after stepping to 1.2 V.

Results and Discussions

Synthesis of Metal Nanoparticle. Sodium borohydride ($NaBH_4$) in aqueous solution has widely been exploited for the reductive production of transition metal powder. With the restriction that the surfactant, cosurfactant and oil phase should not react with the $NaBH_4$, all metal salts in aqueous phase can be reduced with $NaBH_4$ to metal powder (containing ~2−5% borides).[25] For example, in the reduction of H_2PtCl_6 or $CoCl_2$ with $NaBH_4$, eqs 1 and 2 are given if borides are ignored:

$$H_2PtCl_6 + NaBH_4 + 4H_2O \rightarrow Pt\downarrow + NaB(OH)_4 + 6HCl + 2H_2\uparrow \quad (1)$$

$$2CoCl_2 + NaBH_4 + 4H_2O \rightarrow 2Co\downarrow + NaB(OH)_4 + 4HCl + 2H_2\uparrow \quad (2)$$

The nanometer-sized water pools of the reverse micelles and their narrow size distributions provide a stabilized environment for the production of platinum and metal (M) nanoparticles of fairly uniform size.

Surface Characterization of Catalyst: XRD. Figure 1 shows the representative XRD powder patterns for Pt/C-, PtCo/C(T, 500)-, PtCr/C(T, 500)-, and PtFe/C(T, 500)-type catalysts. Figure 2 shows powder-pattern lines for the three types of cubic lattices.[31] The faced-centered and body-centered cubic lattices show reflections from only certain planes, whereas a simple cubic lattice gives observed reflections from all the planes.[31] The position and intensity of reference peaks from JCPDS files for Pt and carbon are shown in Table 4. The XRD data for all Pt/C and PtM/C catalysts are summarized in Table 5. Pt/C and the as-synthesized PtM/C (not shown in Figure 1) have chemically disordered fcc structure. The peak at $2\theta = 25°$ corresponds to the diffraction of the Ketjen Black EC-300J carbon.[32] The five major diffraction peaks of platinum for the Pt/C catalyst are at $2\theta = 39.7°$ (111), 46.2° (200), 67.4° (220), 81.2° (311), and 87.3° (222).[33] According to these peaks of platinum and lattice planes (111), (200), (220), (311), and (222), the type of lattice for Pt was face-centered cubic lattice (fcc lattice), so the Pt−Pt distance, d_1, is $a/\sqrt{2}$ (a is the lattice parameter).

The main diffraction peaks shown in Table 5 for the as-synthesized PtM/C catalysts were shifted to a higher angle as compared with the diffraction peaks of the Pt/C catalyst, suggesting that the unit cell dimension of platinum has been decreased by substitution of the smaller Co, Fe, or Cr atom into the Pt lattice. This shift also suggests that the interatomic distance of Pt was decreased due to the substitution of a smaller atom, such as a transition metal, Co, Fe, or Cr, other than platinum.[17,34] The XRD pattern of Pt/C- and the as-synthesized PtM/C-type catalysts could be fitted to a faced-centered cubic phase.[31] The positions of the main peaks of the as-synthesized PtM/C-type catalysts indicate Pt_3Co, Pt_3Fe, and Pt_3Cr alloy formation, as compared with those of Pt.[35−37] After heat treatment, the XRD powder pattern for PtCo/C(T, 500)- and PtCr/C(T, 500)-type catalysts still shows a fcc structure.

The XRD powder pattern for PtFe/C(T, 500)- and PtFe/C(S, 500)-type catalysts show that, according to the positions of these peaks for PtFe/C(T, 500)- and PtFe/C(S, 500)-type catalysts, the PtFe/C-type catalysts heated at 550 °C match those of simple cubic lattice or primitive tetragonal. According to Bragg law, $2d_{hkl} \sin\theta = \lambda$, and the d-spacing formula $1/d_{hkl}^2 = h^2/a^2 + k^2/b^2 + l^2/c^2$, eq 3 will be obtained,

$$\frac{(2\sin\theta)^2}{\lambda^2} = \frac{h^2}{a^2} + \frac{k^2}{b^2} + \frac{l^2}{c^2} \quad (3)$$

where h, k, and l are lattice plane parameters; d_{hkl} is the perpendicular distance between planes; a, b, and c are lattice constants; λ is the X-ray wavelength (1.5406 Å) for CuK_α; and θ is the Bragg angle. For tetragonal structure, $a = b$. Using (111), (200) planes and their 2θ, we can obtain a, b, and c for PtFe/C(T, 500) and PtFe/C(S, 500) catalysts. Due to a, b, and c being similar (shown in Table 5), the structures of the PtFe/C(T, 500) and PtFe/C(S, 500) catalysts can be attributed to simple cubic lattice or primitive tetragonal. Sun and Elkins[20,38] reported FePt nanoparticles prepared using a chemical reduction method. The XRD patterns shown in references 20,38 for the as-synthesized FePt particles and FePt annealed at 600 °C were similar to ours. They claimed that thermal annealing converts the structure of the internal particles from a chemically disordered fcc phase to the chemically ordered face-centered tetragonal (fct) phase for FePt nanoparticles. We do not agree with their explanation. According to the positions of peaks in references 20 and 38, FePt annealed at 600 °C should be attributed to primitive tetragonal. In addition, a tetragonal system does not have a fct lattice type, but rather, only primitive (P) and body centered (I) lattice types according to "The seven crystal systems and 14 Three-Dimensional Bravais Lattice Types".[39,40] As a result, the shortest Pt−Pt distance for PtFe/C(T, 500) and PtFe/C(S, 500) catalysts, d_1, is c (c is the lattice parameter).

The peaks at $2\theta = 47.6°$ for cobalt, $2\theta = 44.7°$ for iron, and $2\theta = 44.4°$ for chromium were not found, suggesting that there was no evidence to indicate the presence of any crystalline metal M phase. There were also no peaks corresponding to any metal M oxide phases. This was probably because the metal M loading was low, and also, any second metal M species present was highly dispersed or was amorphous and therefore could not be detected.

The average crystallite size for the Pt/C and PtM/C catalysts was determined from the peak width Pt(111) because it has the

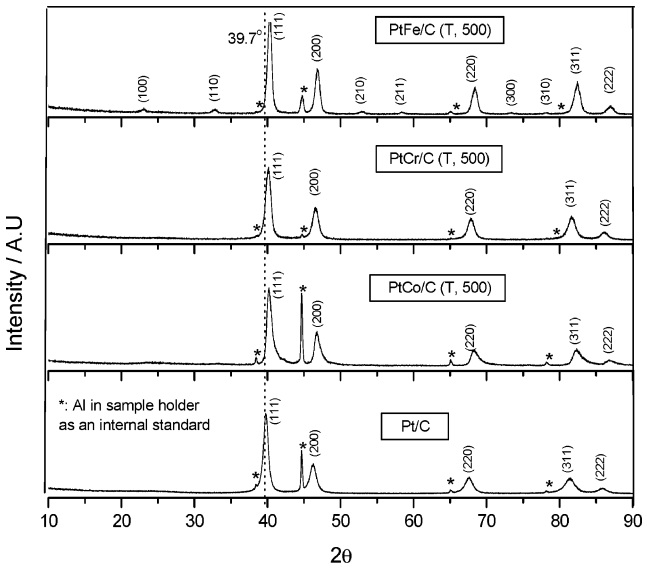

Figure 1. XRD pattern for Pt/C- and PtM/C-type catalysts.

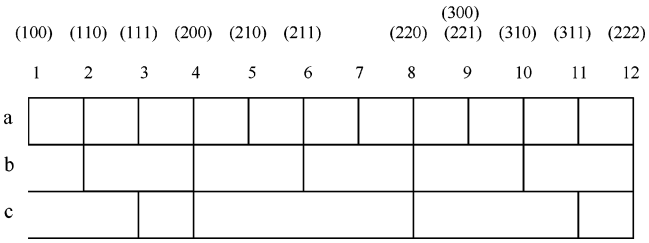

Figure 2. Powder-pattern lines expected for the three types of cubic lattices: (a) simple cubic lattice, (b) body-centered cubic lattice and (c) face-centered cubic lattice.

TABLE 4: XRD Reference Peaks from JCPDS Files

2θ	intensity	analysis	materials
25.0	100	carbon	carbon[32]
39.7	100	Pt(111)	Pt/C[37]
46.2	53	Pt(200)	Pt/C[37]
67.4	31	Pt(220)	Pt/C[37]
81.2	33	Pt(311)	Pt/C[37]

TABLE 5: XRD Data of Pt/C and PtM/C Catalysts

catalyst	lattice types	2θ	crystallite size (nm)[a]	metal area ($m^2\ g^{-1}$)	lattice parameter (Å)	Pt−Pt bond distance (Å)
Pt/C (JCPDS)		39.75			3.92	2.78
Pt/C	fcc	39.75	5.7	50	3.92	2.78
PtCo/C(S)	fcc	40.07	6.6	42	3.89	2.75
PtCo/C(S, 200)	fcc	40.25	6.5	43	3.87	2.74
PtCo/C(S, 500 C)	fcc	40.36	10.6	26	3.87	2.74
PtCo/C(T)	fcc	40.29	5.3	53	3.87	2.74
PtCo/C(T, 200)	fcc	40.33	5.6	50	3.87	2.74
PtCo/C(T, 500)	fcc	40.22	10.5	27	3.88	2.75
PtCr/C(S)	fcc	40.00	10.2	28	3.90	2.76
PtCr/C(S, 200)	fcc	40.03	10.4	27	3.90	2.76
PtCr/C(S, 500)	fcc	40.06	13.2	21	3.89	2.75
PtCr/C(T)	fcc	39.97	8.4	34	3.90	2.76
PtCr/C(T, 200)	fcc	39.98	9.6	30	3.90	2.76
PtCr/C(T, 500)	fcc	40.17	10.5	27	3.88	2.75
PtFe/C(S)	fcc	40.05	4.5	63	3.89	2.75
PtFe/C(S, 200)	fcc	40.09	6.5	44	3.89	2.75
PtFe/C(S, 500)	simple cubic or tetragonal	40.41	12.0	24	$a = b = 3.88$; $c = 3.86$	3.86
PtFe/C(T)	fcc	39.99	5.2	55	3.90	2.76
PtFe/C(T, 200)	fcc	40.00	6.3	45	3.90	2.76
PtFe/C(T, 500)	simple cubic or tetragonal	40.29	12.1	24	$a = b = 3.87$; $c = 3.86$	3.86

[a] Estimated from the fwhm using the Debye−Scherrer equation.

highest intensity value, and was calculated using the Debye−Scherrer equation,[30]

$$T = C\lambda/B\cos\theta \quad (4)$$

where T is the diameter of the average particle size in Å; λ is the X-ray wavelength (1.5406 Å) for CuK_α; θ is the Bragg angle; C is a factor (typically from 0.9 to 1.0) depending on the crystallite shape; and B is the full width at half-maximum, fwhm. For our experiment, $C = 0.9$; $\lambda = 1.5406$ Å. This equation shows an inverse relationship between the crystallite size and the peak profile width: the wider the peak, the smaller the crystallites.

The fourth column in Table 5 shows the crystalline size of the PtM/C-type catalysts. The size is increased as the temperature of heat treatment is raised for all PtM/C catalysts. The crystallite sizes of the as-synthesized PtCo/C and PtFe/C catalysts were small, around 5 or 6 nm after reverse micelle and heat treatment at 200 °C; however, the crystallite sizes of the PtCo/C and PtFe/C catalysts became large (over 10 nm) after heat treatment at 500 °C, suggesting there is sintering at high temperature for the PtCo/C- and PtFe/C-type catalysts. The crystallite size of the PtCr/C catalysts is larger than that of PtCo/C or PtFe/C catalysts after the reverse micelle method, although the preparation conditions for these three catalysts is the same. The aqueous phase in the reverse micelle is $Cr(NO_3)_3$ for the PtCr/C catalyst, but $CoCl_2$ and $FeCl_3$ for the PtCo/C and PtFe/C catalysts, respectively, so we suggest that the larger crystallite size of the PtCr/C catalysts results from the use of $Cr(NO_3)_3$.

Assuming a spherical shape for the particles, the specific area, S ($m^2\ g^{-1}$), for the crystallites was calculated using eq 5,[41]

$$S = 6 \times 10^3\, \rho^{-1} d^{-1} \quad (5)$$

where d is the diameter of the particle (nm) obtained from the XRD, and ρ is the platinum density (21.4 g cm^{-3}). The metal surface is listed in the fifth column of Table 5.

Electron Microscope and Energy Dispersive X-ray Microanalysis. Figure 3 shows scanning electron microscope results of Ketjen Black EC-300J carbon, and a representative as-synthesized PtM/C catalyst, PtCo/C(S). The aim of SEM is to observe supporter, carbon in catalysts. From these images, the spheres correspond to individual particles of Ketjen Black EC-300J carbon. The morphology is composed of integrated particles of sizes around 50 nm. Comparing the image of the Ketjen Black EC-300J carbon with that of the as-synthesized

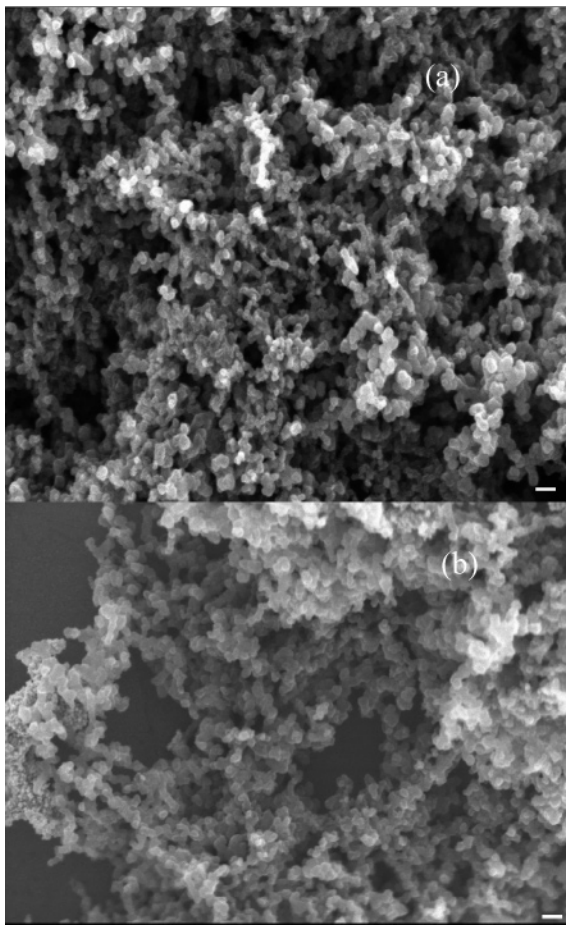

Figure 3. SEM microphotograph of (a) Ketjen Black carbon and (b) PtCo/C(S) catalyst (scale bar: 100 nm).

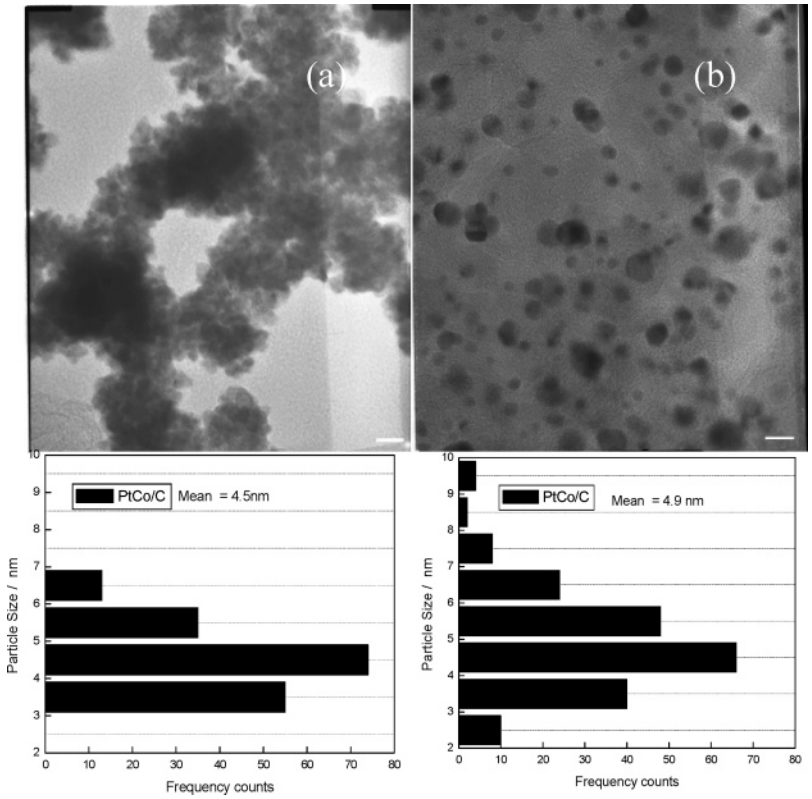

Figure 4. Representative electron micrographs and particle size distribution of PtCo/C catalysts: (a) reverse micelle method and (b) impregnation method (scale bar: 10 nm).

PtCo/C(S) catalyst, it is obvious that the carbon in the as-synthesized PtCo/C(S) catalyst is the same as the Ketjen Black EC-300J carbon, suggesting that the structure and size of the carbon are not changed and that the carbon is less aggregated during the preparation processes of the PtM/C catalysts. It means that the reverse micelle process is a mild process. The metal particles on the carbon could not be seen due to the extremely small size and the technique limitation of SEM.

The size and shape of the metal particles of the catalysts can be characterized using the TEM technique. A representative TEM image and histogram of particle size distribution of the as-synthesized PtM/C prepared using the reverse micelle method are shown in Figure 4a. Every metal nanoparticle is a spherical object. Figure 4b shows a TEM image and histogram of the particle size distribution of the PtCo/C catalyst from UTC fuel cells prepared using an impregnation method. The styles of the metal particles in Figure 4b are different from each other. From Figure 4, the metal particles of the as-synthesized PtM/C prepared using the reverse micelle method are more uniform and have a narrower particle size distribution than those of the PtCo/C prepared using the impregnation method, although there is some low degree of metal particle agglomeration to be observed on the Ketjen Black EC-300J carbon in Figure 4a. The low degree of metal particle agglomeration results from the preparation process, with which the metal nanoparticles were first synthesized during the reverse micelle method, then deposited on Ketjen Black EC-300J carbon. The metal particles of PtCo/C prepared using the impregnation method appear to be well-dispersed on the Ketjen Black EC-300J carbon. This is because the metal particles of the PtCo/C prepared using the impregnation method were obtained by reducing the metal salts and were deposited on the Ketjen Black EC-300J carbon immediately. How the metal nanoparticles were prepared using the reverse micelle method homogeneously and deposited on the carbon is being studied. For example, the supporter, carbon, will be added in the reverse micelle solution before (or while) the reducing solution $NaBH_4$ is being applied. TEM results suggest that the reverse micelle method can control the particle size of the metal and uniformity is practicable.

To confirm the composition of the metal particles, energy dispersive X-ray microanalysis spectra were collected during the TEM and SEM experiments. EDX analysis of the catalysts was performed by reducing the size of the beam and focusing on different areas of the catalysts. Two representative EDX spectra are shown in Figure 5. The catalysts were held on a copper and Al sample holder for the EDX experiment, so the Cu peak at 8.047 eV and the Al peak at 1.5 eV were also observed. On focusing the beam on areas of the Ketjen Black EC-300J carbon of the as-synthesized PtCo/C catalysts, no evidence for platinum and Co metals were found on the carbon support (Figure 5a). Focusing on random metal particle areas of the as-synthesized PtCo/C catalysts, EDX (Figure 5b) shows that the presence of both the Pt and Co metal was observed. The composition of all as-synthesized PtM/C catalysts was also measured by EDX. The results are listed in Table 3. The compositions given in Table 3 do not represent an accurate analysis of the catalysts due to the local nature of the sampling process; however, it shows that both the Pt and M were present on PtM/C catalysts.

Electrochemical Characterization of Catalysts: Cyclic Voltammetry. Figure 6 shows typical steady-state cyclic voltammograms of Pt/C and two of PtM/C catalysts prepared using the reverse micelle method, PtCo/C(T) and PtCo/C(S) in Ar-saturated 1 M $HClO_4$ at 50 mV/s with a Pt loading of ~21 μg Pt/cm^2. Scanning from 0 to 1.2 V versus RHE is called the anodic scan; scanning from 1.2 to 0 V versus RHE is called the cathodic scan. The hydrogen adsorption/desorption features on the Pt/C and PtM/C catalysts between 0.4 and 0 V vs RHE are different from that of a bulk Pt electrode due to the fact

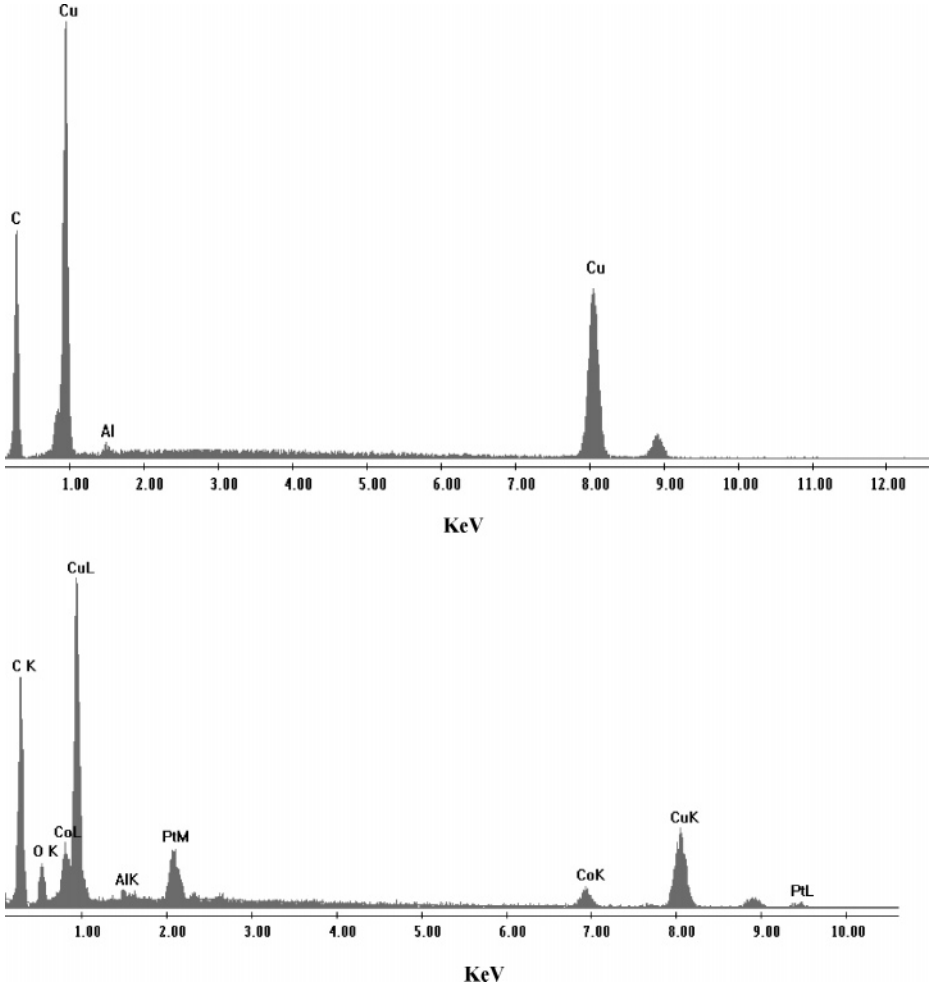

Figure 5. EDX results for Ketjen Black EC-300J carbon and PtCo/C catalysts.

that the carbon-supported Pt particles possess some degree of low-coordinated crystal planes.[42] The comparison of cyclic voltammograms of Pt/C- and PtCo/C(T)- and PtCo/C(S)-type catalysts in Figure 6 shows that the double-layer thickness of the PtCo/C(T)- or PtCo/C(S)-type catalysts is lower than that of the Pt/C catalyst due to addition of Co, although all catalysts used Ketjen Black EC-300J carbon as the support. The onset of the anode oxygen chemisorption and oxide formation on platinum ($Pt + H_2O \rightarrow Pt{-}OH^+ + H^+ + 2e^-$) for the PtCo/C(T)- or PtCo/C(S)-type catalysts is a higher potential than that of Pt/C. For example, the onset of the anode oxygen chemisorption for PtCo/C(T)- or PtCo/C(S)-type catalysts takes place at around 0.85 V relative to 0.70 V of Pt/C catalyst. The difference in oxygen chemisorption and oxide formation of Pt between Pt/C- and PtCo/C(T)- or PtCo/C(S)-type catalysts is attributed to the transition metal, Co. Similar results were obtained for PtFe/C- and PtCr/C-type catalysts (not shown in Figure 6). The transition metals are believed to provide sites to bind and activate water.[43,44] This means that allying with a transition metal effects some changes in the way Pt atoms of PtM/C catalysts interact with water. Thus, the shift in the onset of anode oxygen chemisorption and oxide formation on platinum on the cathodic sweep suggests that there was evidence of Pt/M alloy formation for the PtM/C catalysts. Murthi et al.[42] observed a similar positive shift for Pt/C in 6 M trifluoromethane sulfonic acid (CH_3SO_3H) or PtCo/C in 1 M CH_3SO_3H, as compared to Pt/C in 1 M CH_3SO_3H. They suggest the onset of the oxide formation can be shifted by either alloying the Pt with a second metal that increases the 5d-band vacancies or by lowering the activity of the water.[42]

The charges of hydrogen adsorption at cathodic scan or oxidation of hydrogen at anodic scan were calculated from integration of the hydrogen adsorption or oxidation of hydrogen peaks. These charges can be used to calculate the actual area of the surface Pt in meters squared per gram if the platinum loading on GC RDE surface is known, assuming a correlation value of 210 $\mu C/cm^2$.[43] For hydrogen adsorption ($Pt + H^+ + e^- \rightarrow Pt{-}H_{ads}$) or oxidation of hydrogen ($Pt{-}H_{ads} \rightarrow Pt + H^+ + e^-$), we assume that one electron is passed per platinum site, and therefore, the Pt electrochemical area (ECA) can be calculated by

$$\text{ECA } (m^2\ g^{-1}\ Pt) = \text{hydrogen charge } (\mu C)/(210\ (\mu C/cm^2) \times \text{Pt loading (g)}) \times 10^{-4}$$

The electrochemical surface area (ECA) of Pt/C-, and all the PtM/C-type catalysts are tabulated in Table 6. It can be seen that the PtM/C catalysts had a lower Pt surface area than the monometallic Pt/C catalyst in all cases. This was expected because some Pt surface atoms are covered by Fe, Co, or Cr atoms. ECA of the PtM/C catalysts decreased in each type as the heat treatment temperature increased. These results suggest that the Pt surface area was decreased under high temperature due to some agglomeration. The results are in agreement with that of XRD (in the fifth column of Table 5).

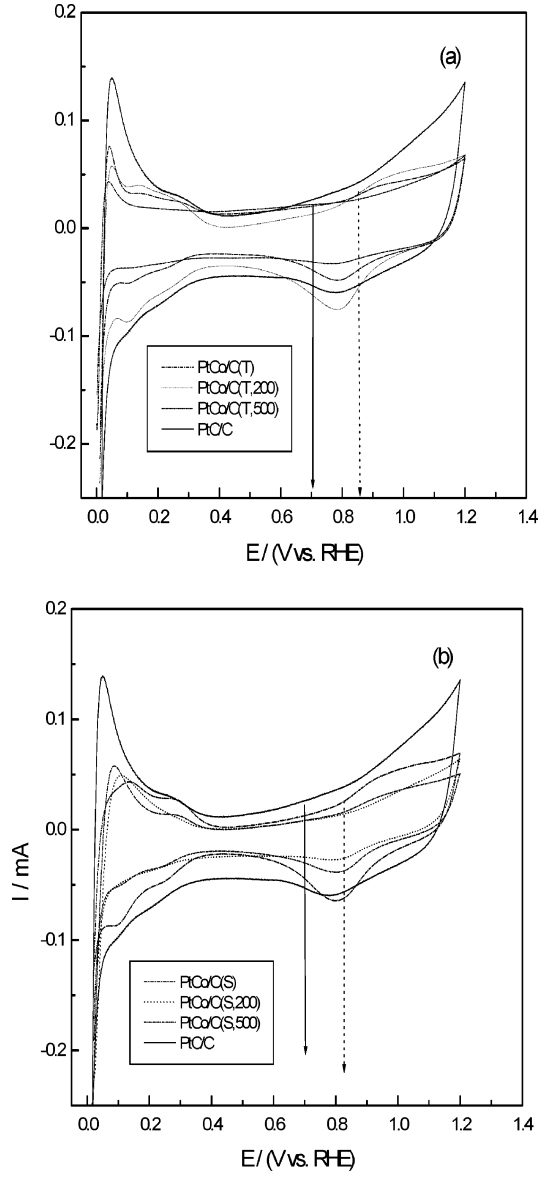

Figure 6. Cyclic voltammetry of (a) PtCo/C(T)- and (b) PtCo/C(S)-type catalysts at room temperature in Ar-saturated 1 M $HClO_4$ at 50 mV/s.

TABLE 6: Electrode Kinetic Parameters for Different Catalysts in 1 M $HClO_4$ at Room Temperature. Scan Rate: 25 mV s^{-1}, Rotation Rate: 1200 rpm.

		j_k, mA/cm^2			
catalysts	ECA, m^2/g	at 0.9 V	at 0.85 V	at 0.8 V	Tafel slope
Pt/C	62	0.019	0.062	0.227	143/77
PtCo/C(T)	52	0.029	0.138	0.536	139/72
PtCo/C(T, 200)	45	0.038	0.183	0.998	131/70
PtCo/C(T, 500)	25	0.116	0.319	0.986	119
PtCo/C(S)	56	0.067	0.376	1.442	147/78
PtCo/C(S, 200)	30	0.050	0.267	1.133	145/71
PtCo/C(S, 500)	30	0.024	0.100	0.471	129/68
PtCr/C(T, 500)	27		0.019	0.0622	117
PtCr/C(S)	47	0.036	0.146	0.615	129/67
PtFe/C(T, 500)	37		0.022	0.0567	116
PtFe/C(S)	55	0.023	0.0776	0.2545	147/77

Evaluation of Catalytic Activity Using the RDE Technique. Figure 7 shows representative rotating disk electrode data, current density vs potential curves for different rotation rates, obtained on a PtCo/C(T, 500)-type catalyst prepared using the reverse micelle method. This Figure shows a single steep oxygen reduction reaction (ORR) was observed around 0.65 V, and mixed kinetic-diffusion control, diffusion-limited currents were recorded between 0.2 and around 0.6 V. Limiting current density, j_d, was obtained at each rotation rate. Similar results were also obtained for other PtM/C catalysts prepared using the reverse micelle method (not shown here).

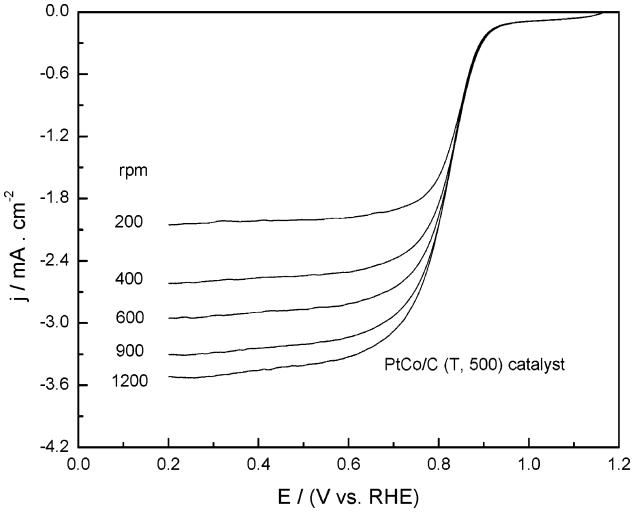

Figure 7. Disk currents obtained during the ORR in the cathodic sweep on Pt/C and PtCo(T, 500) catalysts in O_2-saturated 1 M $HClO_4$ at room temperature. Scan rate: 25 mV s^{-1}.

The electrode was prepared by mixing catalyst with Nafion (only as a binder). The electrode film deposited on the GC RDE such that the Pt or Pt/M exposed in the surface are sufficient for neglecting any important diffusion resistance contribution of the catalyst layer. As described in publications 45 and 46, the resistance of the Nafion film that covers the supported catalysts is sufficiently small. Therefore, the kinetic current densities can generally be adjusted to the simple Koutecky−Levich first-order reaction equation without further need for additional terms,[47]

$$\frac{1}{j} = \frac{1}{j_k} + \frac{1}{j_d} = \frac{1}{j_k} + \frac{1}{B\omega^{1/2}} \tag{6}$$

where j_k is the kinetic current density, j_d is the diffusion-limited current density, ω is the angular frequency of rotation, $\omega = 2\pi f/60$, and f is the RDE rotation rate in rpm. The B parameter is defined as[47,48]

$$B = 0.620nFD^{2/3}\nu^{-1/6}C_O \tag{7}$$

Figure 8 shows j^{-1}-vs-$\omega^{-1/2}$ plots (Koutecky−Levich plots) for oxygen reduction at Pt/C- and PtCo/C(T)-type catalysts. Calculation was performed for n, the number of exchanged electrons, using the slope of the plot and the following values:[49,50] F is the Faraday constant (96 485 C mol^{-1}), D is the diffusion coefficient of the molecular O_2 in 1 M $HClO_4$ solution (1.9×10^{-5} cm^2 s^{-1}), ν is the kinematic viscosity (9.87×10^{-3} cm^2 s^{-1}), and C_O is the concentration of molecular oxygen (1.6×10^{-6} mol cm^{-3}). Table 7 lists the number of exchanged electrons for Pt/C- and PtCo/C(T)-type catalysts. In the diffusion control range, straight lines are obtained. The number of exchanged electrons, n, is 4.2 for Pt/C. The result with $n \approx 4$ for Pt/C suggests that the oxygen reduction proceeds by an overall four-electron-transfer process on the Pt/C catalyst. The value of n for PtCo/C(T) was smaller than that on Pt/C. Coutanceau et al.[51] reported oxygen reduction at Pt nanoparticles in a polyaniline film supported on a GC RDE immersed in O_2-

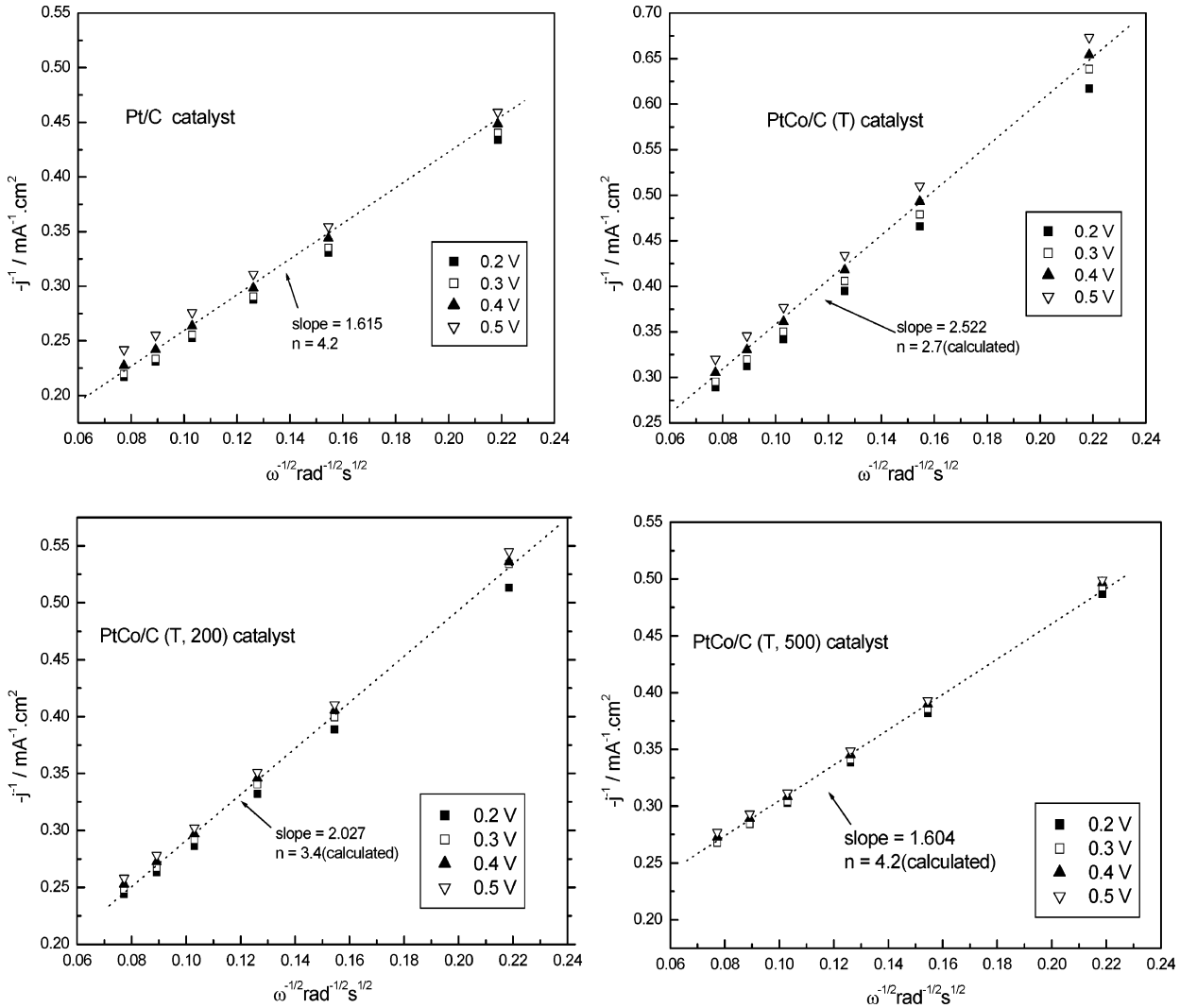

Figure 8. Koutecky−Levich plots at different potentials for ORR in the cathodic sweep on Pt/C- and PtCo/C-type catalysts in O_2-saturated 1 M $HClO_4$ at room temperature. Scan rate: 25 mV s^{-1}.

TABLE 7: The Number of Exchanged Electron in Oxygen Reduction

catalyst	n
Pt/C	4.2
PtCo/C(T)	2.7
PtCo/C(T, 200)	3.4
PtCo/C(T, 500)	4.2

saturated 0.5 M H_2SO_4. They observed that the value of *n* for low platinum loading and high platinum loading was 3 and 4, respectively. In the low platinum loading case, as much of hydrogen peroxide as water is formed by the oxygen reduction reaction. Considering the mechanism of O_2 reduction,[52] the reduction of *n* from 4 can occur when part of the H_2O_2 is generated in the two-electron reduction in the series pathway without further reduction to H_2O. Due to the fact that the transition metals are believed to provide sites to bind and activate water,[43,44] part of the H_2O generated under oxygen reduction was not transferred to the outside of the PtCo/C(T) catalyst. This would lead part of the H_2O_2, the intermediate product of oxygen reduction, not to further reduce to H_2O. Thus, the smaller *n* is observed for oxygen reduction at the PtCo/C(T) catalyst. After heat treatment of the PtCo/C(T) at different temperatures, PtCo/C(T, 200) and PtCo/C(T, 500) catalysts were obtained. The Co in PtCo/C(T, 200) and PtCo/C(T, 500) catalysts contacted Pt much more closely than that in PtCo/C(T) catalyst or even entered into the structure of the Pt, so the ability of adsorbing H_2O for the Co in PtCo/C(T, 200) and PtCo/C(T, 500) catalysts is very low. The larger *n* observed for oxygen reduction on PtCo/C(T, 200) and PtCo/C(T, 500) than on PtCo/C(T) was therefore caused by a further reduction of H_2O_2 to H_2O. As the heat treatment temperature was increased, the number of exchanged electrons, *n*, was found to increase.

Mass transport corrected Tafel plots of j_k for oxygen reduction are shown in Figure 9 for Pt/C-, PtCo/C(S)-, and PtCo/C(T)-type catalysts at 1200 rpm. Tafel plots (*E* vs $\log|j_k|$) can be directly extracted from experimental data and eq 8:

$$j_k = \frac{j_d \times j}{j_d - j} \tag{8}$$

Schmidt and Mailard recently used a thin-film RDE or porous RDE method to investigate the catalytic activity of carbon-supported Pt catalysts for oxygen reduction reaction toward fuel cell reactions.[22,46,53] In the thin-film RDE or porous method, a glassy carbon disk is successively covered by two layers; namely, an inner layer of catalyst and an outer layer of Nafion. It means that O_2 coming from the solution first diffuses through a Nafion film and then reacts at the catalyst surface. This situation of the thin-film or porous RDE is very similar to that of the so-called "thin-film model" of fuel cell electrodes. Thus,

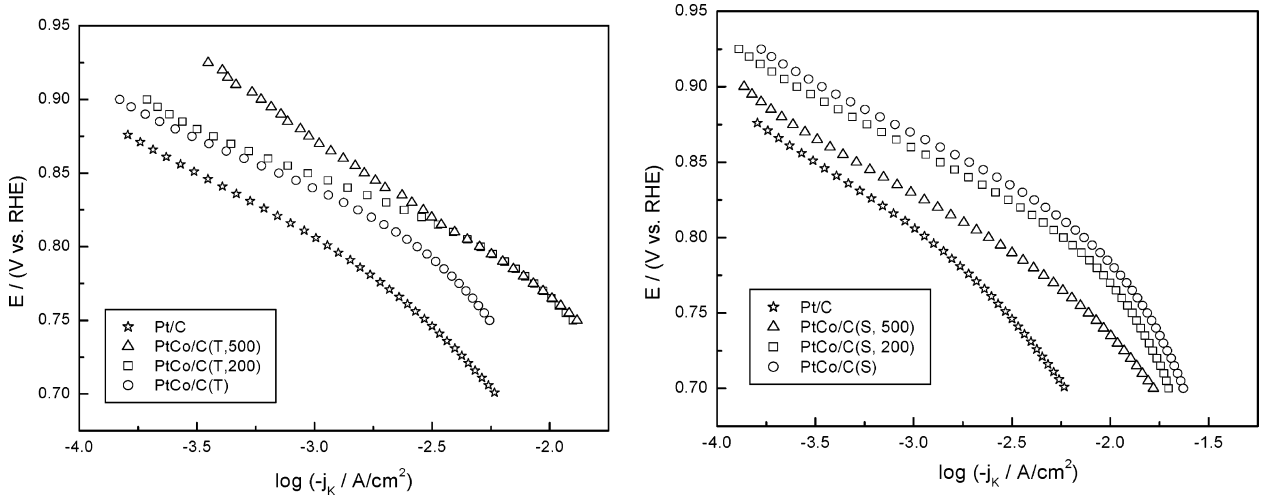

Figure 9. Tafel plots of j_k for ORR obtained from disk current in the cathodic sweep at 1200 rpm on Pt/C- and PtCo/C-type catalysts.

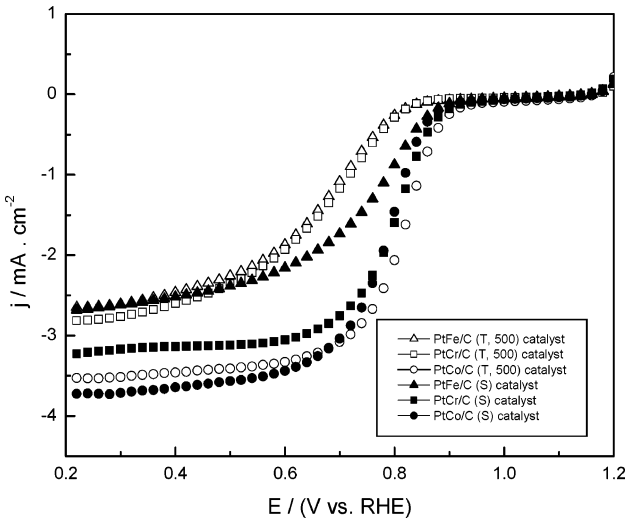

Figure 10. Disk currents obtained during the ORR in the cathodic sweep in O_2-saturated 1 M $HClO_4$ at room temperature. Scan rate, 25 mV s^{-1}; rotation rate, 1200 rpm.

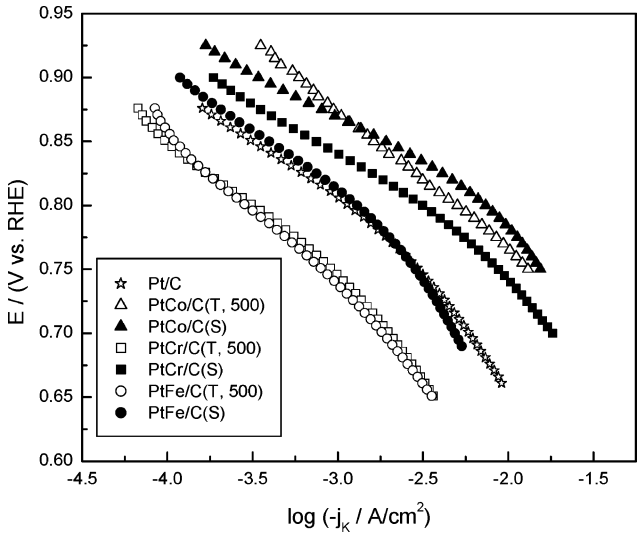

Figure 11. Tafel plots of j_k for ORR obtained from disk current in the cathodic sweep at 1200 rpm on Pt/C-, PtM/C(S)-, and PtM/C(T, 500)-type catalysts.

in our work, j_k can be considered as an indicator of catalytic activity. As heat treatment increased from Figure 9, the increase in $-j_k$ for the PtCo/C(T)-type catalyst and decrease in $-j_k$ for the PtCo/C(S)-type was observed. Heat treatment is not useful for the simultaneous reaction procedure of the reverse micelle method, suggesting that the Pt atom and the Co atom have been in close contact for the as-synthesized PtCo/C(S) catalyst. It is important for the sequential reaction procedure of the reverse micelle method to heat the as-synthesized PtCo/C(T), probably because Pt was coated on the Co surface after the formation of Co nanoparticles. In order to form a Pt/Co alloy or make Pt and Co come in close contact, heat treatment is needed for the as-synthesized PtCo/C(T)-type catalyst. The same result was also obtained for the PtFe/C and PtCr/C catalysts (not shown in Figure 9). As a result, the order of catalytic activity for ORR was PtM/C(T, 500) > PtM/C(T, 200) > PtM/C(T) using the sequential reaction procedure of the reverse micelle method and PtM/C(S) > PtM/C(S, 200) > PtM/C(S, 500) using the simultaneous reaction procedure of the reverse micelle method.

To compare catalytic activity for oxygen reduction on different types of catalysts, Figure 10 shows RDE results at 1200 rpm for the PtM/C(T, 500)- and PtM/C(S)-type catalysts, and Figure 11 shows their mass transport corrected Tafel plots of j_k compared with the Pt/C catalyst at 1200 rpm. Table 6 shows the kinetic data for all PtM/C catalysts. It is obvious that the PtCo/C catalyst has best activity for oxygen reduction. From Figure 11, even though it is clear that the Tafel slope for the oxygen reduction reaction is changing continuously in the potential range examined,[54,55] two Tafel regions at low and high overpotential were found for Pt/C and PtM/C(S) catalysts. The Tafel slopes for the Pt/C and PtM/C(S) catalysts were well-defined around RT/F (~60 mV/decade) for the low overpotential range (E > 0.85 V) and 2RT/F (~120 mV/decade) for the high overpotential range (E < 0.80 V), although some are slightly different. They are in good agreement with Tafel slopes reported in the literature for single-crystal Pt electrodes,[56] polycrystalline Pt,[57] and carbon-supported Pt catalysts.[58] The appearance of two linear segments in the Tafel plot has typically been reported for the O_2 reduction reaction on platinum electrode in acidic medium and at the platinum/Nafion interface. Variations in the Tafel slopes are attributed to the influence of different adsorption and rate-determining steps over the potential ranges investigated.[56−58] However, a single Tafel slope of ~120 mV/decade was observed for PtM/C(T, 500) catalysts in the entire mixed activation-diffusion region, which is indicative of total Pt/M alloy formation for PtM/C(T, 500) catalysts.[42] Comparing the seven catalysts in Figure 11, the trend of catalytic activity for oxygen reduction reaction is PtCo/C(T, 500) ~ PtCo/C(S) > PtCr/C(S) > PtFe/C(S) ~ Pt/C > PtFe/C(T, 500) ~ PtCr/C(T, 500). The

trend implies that catalytic activity of ORR is dependent on more than Pt alloying with transition metals. For example, Mukerjee[6] showed that the enhanced electrocatalysis exhibited by binary Pt alloys appears to originate primarily as a result of changes in the lattice structure owing to alloying. Huang explained that the enhancement in the ORR activity on the Pt-based alloy catalyst is generally correlated to the change in the Pt−Pt interatomic distance.[59] However, we think that many other factors also affect the catalytic activity of ORR. These factors include the catalyst preparation method; reaction conditions, and choice of transition metal for a certain preparation method; the size of the metal particle; and the relation between platinum and the other metals. For example, in this paper, two reaction procedures (sequential and simultaneous) give a different order of catalytic activity for the heat treatment temperature. For the sequential reaction procedure, two metals, Pt and M, were deposited on the support at different times, so the heat treatment is important for the formation of the PtM alloy. However, for the simultaneous reaction procedure, Pt and M were in close contact while they were deposited on support for the as-synthesized PtM/C(S), so too high a temperature will result in the formation of big metal particles, although the PtM alloy will also form then.

Conclusions

We have reported synthesis of PtM nanoparticles by reducing H_2PtCl_6 and M salts (M = Co, Cr, or Fe) in a reverse micelle system and preparation of PtM/C catalysts by depositing the PtM nanoparticles on carbon (on Ketjen Black EC-300J). PtM/C catalysts were characterized by different surface techniques. The results showed that PtM particles on PtM/C catalysts prepared using the reverse micelle method were nanoscale and more uniform and had a narrower particle size distribution than that prepared using the impregnation method. Catalytic activities for the oxygen reduction reaction on PtM/C catalysts were evaluated by the RDE technique. The results indicated that PtCo/C(T, 500) and PtCo/C(S) catalysts possess better catalytic activity for the oxygen reduction reaction than Pt/C and other Pt bimetallic catalysts in our reverse micelle system. The result of the trend of catalytic activity for the oxygen reduction reaction (PtCo/C(T, 500) ∼ PtCo/C(S) > PtCr/C(S) > PtFe/C(S) ∼ Pt/C > PtFe/C(T, 500) ∼ PtCr/C(T, 500)) suggested that heat treatment was needed for catalyst preparation using the sequential reduction procedure, and high temperature was not good for catalyst preparation using simultaneous reduction in our reverse micelle method. All the above-mentioned results implied that many factors influenced the catalytic activity of the oxygen reduction reaction, including Pt alloying with transition metals, choice of the transition metal for certain preparation method, and catalyst preparation conditions.

Acknowledgment. The authors gratefully acknowledge financial support from the Army Research Office under a single investigator award. We thank Michael Frongillo of MIT for TEM measurements. One of the authors (Y.Q.) thanks J. M. Ziegelbauer, V. S. Murthi, and Y. Garsany of Northeastern University for valuable advice and discussions regarding the RDE experiment and data analysis.

References and Notes

(1) Hoogers, G. *Catalysts for the Proton Exchange Membrane Fuel Cell*; CRC Press: Boca Raton, FL, 2003.
(2) Bregoli, L. J. *Electrochim. Acta* **1978**, *23*, 489.
(3) Bett, J.; Lundquist, J.; Washington, E.; Stonehart, P. *Electrochim. Acta* **1973**, *18*, 343.
(4) Landsman, D. A.; Luczak, F. J. U.S. Patent 4,316,944, 1982.
(5) Luczak, F. J.; Landsman, D. A. U.S. Patent 4447506, 1984.
(6) Mukerjee, S.; Srinivasan, S. *J. Electroanal. Chem.* **1993**, *357*, 201.
(7) Jalan, V.; Taylor, E. J. *J. Electrochem. Soc.* **1983**, *130*, 2299.
(8) Glass, J. T.; Cahen, G. L., Jr.; Stoner, G. E. *J. Electrochem. Soc.* **1987**, *134*, 58.
(9) Paffett, M. T.; Beery, J. G.; Gottesfeld, S. *J. Electrochem. Soc.* **1988**, *135*, 1431.
(10) Beard, B. C.; Ross, P. N., Jr. *J. Electrochem. Soc.* **1990**, *137*, 3368.
(11) Appleby, A. J. *Energy* **1986**, *11*, 13.
(12) Jalan, V. M. J. U.S. Patent 4192907, 1980.
(13) Itoh, T.; Katoh, K. U.S. Patent 5024905, 1991.
(14) Itoh, T.; Kato, K. U.S. Patent 5096866, 1992.
(15) Tsurumi, K.; Nakamura, T.; Sato, A. U.S. Patent 4985386, 1991.
(16) Stonehart, P. U.S. Patent 5593934, 1997.
(17) Hwang, J. T.; Chung, J. S. *Electrochim. Acta* **1993**, *38*, 2715.
(18) Neergat, M.; Shukla, A. K.; Gandhi, K. S. *J. Appl. Electrochem.* **2001**, *31*, 373.
(19) Sun, S.; Anders, S.; Thomson, T.; Baglin, J. E. E.; Toney, M. F.; Hamann, H. F.; Murray, C. B.; Terris, B. D. *J. Phys. Chem. B* **2003**, *107*, 5419.
(20) Sun, S.; Murray, C. B.; Weller, D.; Folks, L.; Moser, A. *Science* (Washington, D. C.) **2000**, *287*, 1989.
(21) Zhang, X.; Chan, K.-Y. *J. Mater. Chem.* **2002**, *12*, 1203.
(22) Schmidt, T. J.; Gasteiger, H. A.; Stab, G. D.; Urban, P. M.; Kolb, D. M.; Behm, R. J. *J. Electrochem. Soc.* **1998**, *145*, 2354.
(23) Paulus, U. A.; Endruschat, U.; Feldmeyer, G. J.; Schmidt, T. J.; Bonnemann, H.; Behm, R. J. *J. Catal.* **2000**, *195*, 383.
(24) Carpenter, E. E. *J. Magn. Magn. Mater.* **2001**, *225*, 17.
(25) Boennemann, H.; Brijoux, W.; Brinkmann, R.; Fretzen, R.; Joussen, T.; Koeppler, R.; Korall, B.; Neiteler, P.; Richter, J. *J. Mol. Catal.* **1994**, *86*, 129.
(26) Lin, J.; Zhou, W.; Kumbhar, A.; Wiemann, J.; Fang, J.; Carpenter, E. E.; O'Connor, C. J. *J. Solid State Chem.* **2001**, *159*, 26.
(27) Giannakas, A. E.; Ladavos, A. K.; Pomonis, P. J. *Appl. Catal., B* **2004**, *49*, 147.
(28) Pileni, M. P. *Langmuir* **1997**, *13*, 3266.
(29) Wu, M.-L.; Chen, D.-H.; Huang, T.-C. *Langmuir* **2001**, *17*, 3877.
(30) Cullity, B. D. *Elements of X-ray diffraction*, 2nd ed.;, Addision-Wesley Publishing Company, 1978.
(31) Laidler, K. J.; Meiser, J. H.; Sanctuary, B. C. *Physical Chemistry* 4th ed.; Houghton Mifflin Company: Boston, 2003.
(32) Arico, A. S.; Antonucci, V.; Giordano, N.; Shukla, A. K.; Ravikumar, M. K.; Roy, A.; Barman, S. R.; Sarma, D. D. *J. Power Sources* **1994**, *50*, 295.
(33) JCPDS International Center for Diffraction Data, U.S.A. Powder Diffraction Files (Inorganic Volumes); 4-802.
(34) Arico, A. S.; Shukla, A. K.; El-Khatib, K. M.; Creti, P.; Antonucci, V. *J. Appl. Electrochem.* **1999**, *29*, 671.
(35) JCPDS International Center for Diffraction Data, U.S.A. Powder Diffraction Files (Inorganic Volumes); *29-1423*.
(36) JCPDS International Center for Diffraction Data, U.S.A. Powder Diffraction Files (Inorganic Volumes); 34−1080.
(37) JCPDS International Center for Diffraction Data, U.S.A. Powder Diffraction Files (Inorganic Volumes); 29−499.
(38) Elkins, K. E.; Vedantam, T. S.; Liu, J. P.; Zeng, H.; Sun, S.; Ding, Y.; Wang, Z. L. *Nano Lett.* **2003**, *3*, 1647.
(39) Smart, L. E.; Moore, E. A. *Solid State Chemistry*, 2nd ed.; Stanley Thornes: Cheltenham, 1998.
(40) West, A. R. *Solid State Chemistry and its Applications*; Wiley: New York, Chichester, 1990.
(41) Stonehart, P. *J. Appl. Electrochem.* **1992**, *22*, 995.
(42) Murthi, V. S.; Urian, R. C.; Mukerjee, S. *J. Phys. Chem. B* **2004**, *108*, 11011.
(43) Crabb, E. M.; Marshall, R.; Thompsett, D. *J. Electrochem. Soc.* **2000**, *147*, 4440.
(44) Markovic, N. M.; Widelov, A.; Ross, P. N.; Monteiro, O. R.; Brown, I. G. *Catal. Lett.* **1997**, *43*, 161.
(45) Paulus, U. A.; Wokaun, A.; Scherer, G. G.; Schmidt, T. J.; Stamenkovic, V.; Markovic, N. M.; Ross, P. N. *Electrochim. Acta* **2002**, *47*, 3787.
(46) Paulus, U. A.; Schmidt, T. J.; Gasteiger, H. A.; Behm, R. J. *J. Electroanal. Chem.* **2001**, *495*, 134.
(47) Duron, S.; Rivera-Noriega, R.; Nkeng, P.; Poillerat, G.; Solorza-Feria, O. *J. Electroanal. Chem.* **2004**, *566*, 281.
(48) Pleskov, Y. V., Filinovskii, V. Y., Eds. *The Rotating Disk Electrode*; Plenum Press: New York, 1976.
(49) Hsueh, K. L.; Gonzalez, E. R.; Srinivasan, S. *Electrochim. Acta* **1983**, *28*, 691.
(50) Maruyama, J.; Abe, I. *Electrochim. Acta* **2003**, *48*, 1443.
(51) Coutanceau, C.; Croissant, M. J.; Napporn, T.; Lamy, C. *Electrochim. Acta* **2000**, *46*, 579.

(52) Maruyama, J.; Inaba, M.; Morita, T.; Ogumi, Z. *J. Electroanal. Chem.* **2001**, *504*, 208.
(53) Maillard, F.; Martin, M.; Gloaguen, F.; Leger, J. M. *Electrochim. Acta* **2002**, *47*, 3431.
(54) Grgur, B. N.; Markovic, N. M.; Ross, P. N. *Can. J. Chem.* **1997**, *75*, 1465.
(55) Damjanovic, A.; Sepa, D. B. *Electrochim. Acta* **1990**, *35*, 1157.
(56) Takasu, Y.; Fujii, Y.; Yasuda, K.; Iwanaga, Y.; Matsuda, Y. *Electrochim. Acta* **1989**, *34*, 453.
(57) Gojkovic, S. L.; Zecevic, S. K.; Savinell, R. F. *J. Electrochem. Soc.* **1998**, *145*, 3713.
(58) Jiang, J.; Kucernak, A. *Electrochem. Solid-State Lett.* **2000**, *3*, 559.
(59) Huang, Q.; Yang, H.; Tang, Y.; Lu, T.; Akins, D. L. *Electrochem. Commun.* **2006**, *8*, 1220.